AD-A282 831

ATION PAGE

Form Approved
OMB No. 0704-0188

1. 06/21/94

3. REPORT TYPE AND DATES COVERED
Final 05/14/93 through 05/14/94

4. TITLE AND SUBTITLE
Optically Controlled MMW Beamsteering Beamforming Antenna

5. FUNDING NUMBERS
C: N00014-93-C-0116

6. AUTHOR(S)
Lev Sadovnik

7. PERFORMING ORGANIZATION NAME(S) AND ADDRESS(ES)
Physical Optics Corporation
20600 Gramercy Place, Building 100
Torrance, California 90501

8. PERFORMING ORGANIZATION REPORT NUMBER
3219

9. SPONSORING / MONITORING AGENCY NAME(S) AND ADDRESS(ES)
Office of Naval Research
Code 4414 (1264)
800 North Quincy Street, BT #1
Arlington, VA 22217-5660

10. SPONSORING / MONITORING AGENCY REPORT NUMBER

11. SUPPLEMENTARY NOTES

12a. DISTRIBUTION / AVAILABILITY STATEMENT
Unlimited

13. ABSTRACT *(Maximum 200 words)*

In this research project, Physical Optics Corporation (POC) has developed theoretical and laboratory models of semiconductor waveguides for MMW antennas. The physical model has been tested experimentally demonstrating attenuation of MMW propagation in the semiconductor waveguide. POC has also investigated coupling between semiconductor and metal waveguides. A new type of evanescent-coupling scanning antenna has been demonstrated and tested. The results of this project form the foundation for the fabrication of a light controlled antenna.

14. SUBJECT TERMS
MMW Antenna, Semiconductor Waveguide

15. NUMBER OF PAGES
31

16. PRICE CODE

17. SECURITY CLASSIFICATION OF REPORT	18. SECURITY CLASSIFICATION OF THIS PAGE	19. SECURITY CLASSIFICATION OF ABSTRACT	20. LIMITATION OF ABSTRACT
Unclassified	Unclassified	Unclassified	SAR

NSN 7540-01-280-5500

Standard Form 298 (Rev. 2-89)
Prescribed by ANSI Std Z39-18
298-102

DISCLAIMER NOTICE

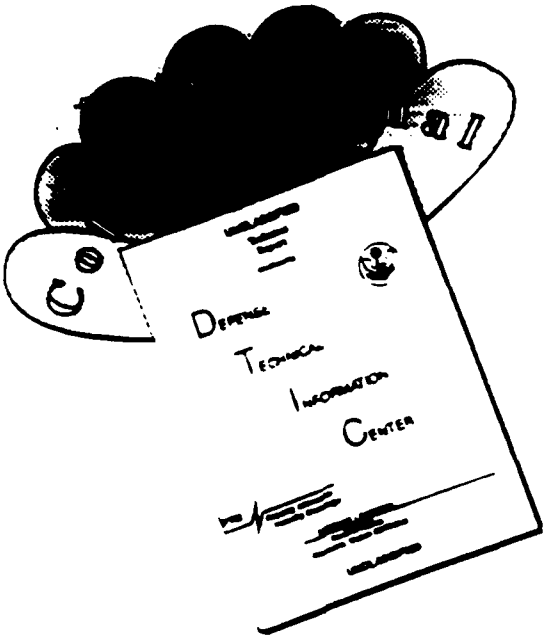

THIS DOCUMENT IS BEST QUALITY AVAILABLE. THE COPY FURNISHED TO DTIC CONTAINED A SIGNIFICANT NUMBER OF COLOR PAGES WHICH DO NOT REPRODUCE LEGIBLY ON BLACK AND WHITE MICROFICHE.

TABLE OF CONTENTS

1.0 INTRODUCTION

The millimeter wave region has a number of well-known advantages making it desirable for use in such applications as guidance, sensing, and communications. These advantages include: a very broad bandwidth, which solves the spectrum crowding problem; a short wavelength, which leads to small, lightweight transmitters, receivers, and antennas; and suitability for use in integrated designs, taking advantage of the inherent features of ruggedness, reproducibility, reliability, and low cost.

A variety of antennas have been designed or are currently under investigation for use in the millimeter wave band. Three classes of millimeter wave antennas can be distinguished. The first consists of well-known configurations such as reflectors, lenses, and horn antennas. The use of these antennas at microwave and lower frequencies is well established. Scaling into the millimeter wave region is straightforward in most cases. Most millimeter wave antennas currently in use belong to this class.

The second class, consisting of antennas with features peculiar to the millimeter wave region, is still under study and is more diverse than the first. It includes radiating structures such as microstrip millimeter wave antennas, antennas using open millimeter waveguides, and integrated antennas. Microstrip antennas have many practical advantages, and have thus found numerous applications in the UHF through microwave bands. Recently, several efforts have been undertaken to extend the operation of these antennas into the millimeter wave region. In these first two classes, scanning must be performed mechanically.

The third class encompasses phased array antennas. It is widely believed that, in the millimeter wave band, a phased array antenna is the only possible means of agile beamforming/beamsteering. A phased array is a network of radiating elements, each of which is primarily non-directional, with a cooperative radiation pattern that is highly directional in shape. The flexibility of electronic steering and beamforming afforded by array antennas comes at the cost of the individual control of each element. The $N \times N$ elements of such antennas are driven with the same signal, each element having a different phase. In practice, a single signal is split equally into $N \times N$ signals to feed the elements, and a phase shifting network, typically using ferrite shifters or diodes, performs the individual phase control of each element [1]. For large arrays (say, $N > 10$), the complexity of the power splitting network and the cost of the $N \times N$ phase shifters can become quite high, to say nothing of the bulkiness of the waveguide plumbing. Moreover, for very large arrays, the

computation required to calculate the array's phase distribution needed to produce the desired radiation pattern is a considerable burden. These are the most serious drawbacks of conventional phased array antenna systems. Another problem with phased arrays for homing applications is that they are difficult and costly to package into an airframe diameter of 150 mm or less.

In addition to these technological drawbacks, the phased array antenna is restricted in its angular sampling. In practice, the exact required phase shift for each phase shifter cannot be attained. The phases are set to a series of discrete values, for example to values of 180°, 90°, 45°, 22.5°, etc. By combining these values, the required scanning angle is approximated as closely as possible. The smaller the number of values available, the larger the resulting error. In a 4-bit phase shifter, only the values 180°, 90°, 45°, and 22.5° are available. The maximum error is ± 11.25°.

Another important consideration for phase shifting elements is their bandwidth. Reflection and loaded-line phase shifters are inherently narrowband. The bandwidth of a true time-delay switched-line phase shifter is limited by the bias circuitry and by resonances in the phase shifter.

High-pass/low-pass type phase shifters can be designed for broader bandwidths. However, this usually entails a large number of diodes or GaAs FETs (typically six or more per bit), which are not necessarily identical [2]. Generally, in any broadband design of a phase shifter, some RF performance must be compromised in one or more of the following characteristics:

- Insertion loss
- Insertion loss flatness
- Insertion mismatch
- Phase versus frequency characteristics
- Circuit complexity.

The optical beamforming network (OBFN) technique is a novel concept which was originally developed [2] to solve some of these problems. Specifically, the computation of the array's phase distribution is performed optically by a combination of a Fourier transform lens and a spatial light modulator, while signals are distributed by fiber optic bundles. For coherent demodulation to yield the proper center frequency, an optical reference beam whose frequency has been offset by the desired RF carrier frequency is needed. Phases computed optically are coherently demodulated to yield the phases for each millimeter wave element. There is an immediate reduction of complexity and cost because millimeter wave power splitting hardware is no longer required. Also, the optical computation of the phase distribution is performed in parallel, which is quite advantageous for very large arrays.

A comprehensive study of optically implemented radar has been conducted by Harris Corporation [3] and Rockwell International Science Center [4] (sponsored by the SDIO and Rome Laboratory). From this study it can be inferred that the central requirement in the design of an OBFN is to develop a technique by which a 1 to 100 GHz frequency offset (the center frequency of the millimeter wave array) can be impressed on an optical carrier. The plausibility of the technique becomes increasingly doubtful as the frequency approaches 100 GHz, so that for a millimeter-wave phased-array antenna the role of the optical components is reduced to the simple distribution of coded control signals to the phase shifters incorporated into a microstrip antenna. The weaknesses of using individual phase controls for each element appear again, now redoubled by the higher packaging density of the millimeter-wave circuitry.

Finally, for the antennas of the third class, their high cost is the single most restrictive constraint on their commercial use. Typical microwave phased arrays consist of 1,000 to 100,000 elements. The cost per element is on the order of $1,000 to $10,000. Clearly, methods of reducing these costs will have a decisive influence on the practical usefulness of such antennas.

2.0 POC CONCEPT

POC has looked at the problem from a different perspective. Rather than imposing a millimeter-wave frequency on a light carrier, the millimeter waves are subjected to direct optical modulation. Two theoretically and experimentally proven premises form the foundation of POC's patented [5] technology. They can be stated as follows:

- The MMW transmittance/reflectance of a semiconductor material can be varied by more than several orders of magnitude by illuminating the material with light whose photon energy is greater than the semiconductor's bandgap.

- Phase shifting is not the only way to control the direction and shape of a MMW beam. MMW beamforming and beamsteering can be achieved through MMW amplitude modulation alone.

POC's novel millimeter wave diffraction concept can be explained with the use of several drawings, starting from a simple conceptual presentation and gradually moving toward a more

complete design. Setting aside the nature of the grating material (assume a metal grating for simplicity), we can state that a grating will diffract a MMW beam according to the equation

$$\sin\varphi + \sin\theta = m\lambda/D \quad , \tag{2-1}$$

where m = 0, ±1, ... is the diffraction order number (m = 0 corresponds to the zeroth order, the undiffracted beam), and D is the grating period (see Figure 2-1). The same diffraction pattern is produced by reflection from a grating (Figure 2-2).

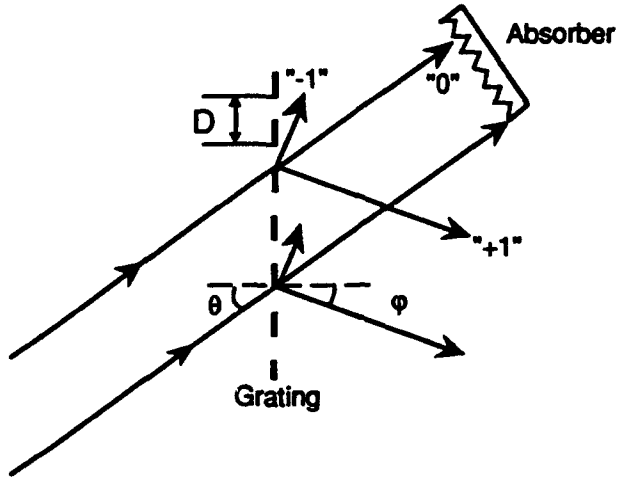

Figure 2-1
MMW diffraction by a transmission grating.

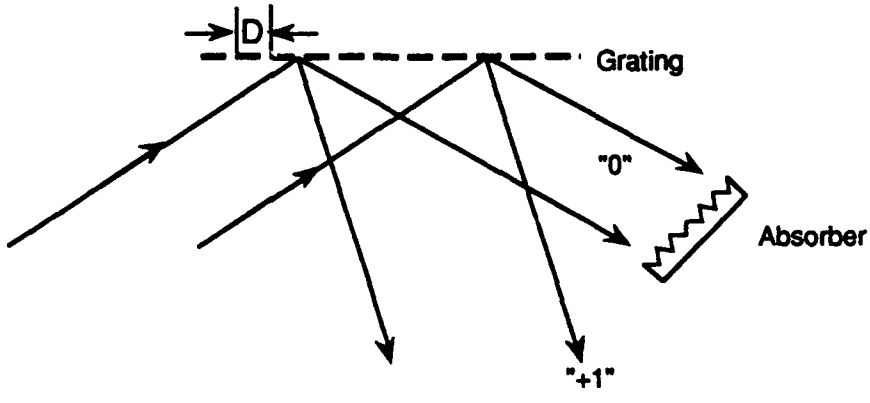

Figure 2-2
MMW diffraction by a reflection grating.

Here, an absorber is introduced to eliminate mirror (Fresnel) reflection, leaving only the diffracted beam. The main conclusion to draw from these two figures is that the direction of an output diffracted beam (for a fixed wavelength and input incidence angle) is determined by the grating period. Varying the grating period steers the MMW diffracted beam in accordance with Eq. (2-1).

In the next step, a very shallow incident beam can be thought of as being confined in a waveguide (Figure 2-3), so that a grating can couple it out. Once again, the direction of the output beam varies with the grating period D. Although in a single-mode waveguide MMWs do not really reflect from boundaries, their behavior is described by

$$\sin\varphi = n_{eff} - \frac{\lambda}{D} \quad , \qquad (2\text{-}2)$$

where n_{eff} is the waveguide's effective refractive index. Again, controlling the grating parameters controls, the amplitude and phase of the MMW antenna field as well.

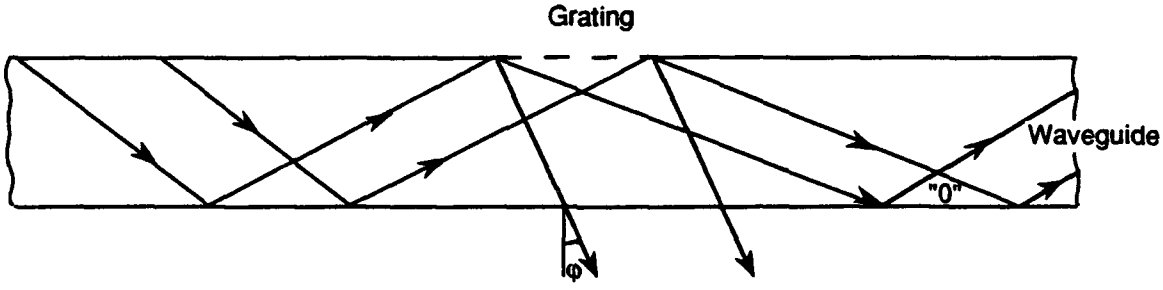

Figure 2-3
Waveguide grating coupler geometry.

This principle, in a more elaborate form, constitutes the foundation for POC's Guided-wave Antenna Induced by Light (GAIL). **The main idea is to couple MMW radiation out of a semiconductor waveguide into free space using a grating coupler induced by light.** This is similar to a slot array which leaks radiation from a traveling wave antenna or an array of metal strips in a microstrip antenna design. The difference is that, in contrast to those antennas, GAIL has the flexibility to rapidly change its radiation pattern, and is thus capable of agile beamsteering and beamforming.

It should be noted that, by the reciprocity principle, an antenna that emits radiation in a certain direction will also receive radiation preferentially from that direction. Thus, the proposed antenna can function both as an agile directional emitting antenna and as an agile directional receiving antenna.

3.0 PROJECT RESULTS

3.1 Theoretical Aspects of GAIL

Three theoretical issues strongly affect the GAIL antenna design: conditions for a single mode waveguide grating coupler, the efficiency of the grating coupler, and the effect of nonstationary (pulsed) illumination on antenna efficiency.

Most millimeter waveguides are open guiding structures; to minimize structural complexity and conduction losses, the guided fields are not enclosed on all sides by metal walls. This means that if the uniformity of the guiding structure is perturbed, or the guide is not excited in the appropriate mode, radiation will occur and part of the guided energy will leak out of the waveguide. This leakage effect can be used to advantage in the antenna design. Intentionally introduced perturbations in an open waveguide permit the control of leaking radiation. Typical antennas of this kind are leaky-wave antennas or modified surface-wave antennas. Like the guides from which they are derived, they are structurally simple and easy to fabricate; they are directly compatible with the guides and suitable for integrated designs; moreover, the use of guiding materials such as silicon permits monolithic integration with MMW ICs.

The key parameters in the antenna design are the operating frequency, the guide wavelength, and the perturbation spacing.

The operating frequency of a system is governed by the requirements imposed by the application: resolution, range, and size of components. In a more practical sense, it depends on the availability of small, rugged, and reliable millimeter-wave power sources which have sufficient power output for the intended application. The primary solid-state sources used to date have been Gunn and IMPATT diodes. We have, therefore, chosen to limit the GAIL design to operation at 90 GHz, where adequate test equipment and power sources are available.

The guide wavelength for a given material and frequency is determined by the physical size of the guide. It is advantageous from a practical point of view to avoid multisignal complexity as much as possible. Single-mode operation must be maintained in the propagation of energy in the waveguide so that only a single beam will radiate from the antenna.

Let us assume that, because of its size, the silicon slab is a single-mode planar waveguide, supporting only one transverse-electric (TE) wave. The geometry of the field distribution in a rectangular waveguide is shown in Figure 3-1.

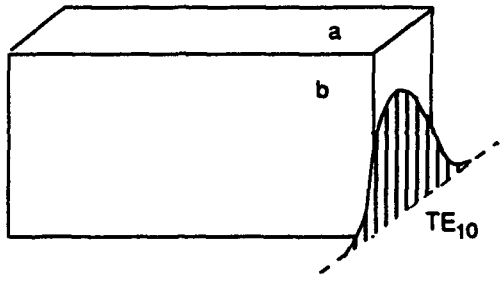

Figure 3-1
Field distribution of the dominant TE_{10} mode in a rectangular waveguide.

The dominant TE_{10} mode is, in general, degenerate and hence may couple at any discontinuity or imperfection. This is important for grating antenna applications.

Ideally, the waveguide should be as large as possible for any given frequency of operation since this eases fabrication and lessens the effect of size variation on the guide wavelength and scan angle. The maximum waveguide thickness is defined as that above which multiple modes can propagate.

The waveguide is single-mode when $(a/\lambda_0)\ NA < 1$, where a is the thickness, λ_0 is the free-space wavelength, and NA is the numerical aperture, $NA = \sqrt{n^2 - 1}$, $n = 3.43$ is the refractive index of silicon. Unlike metal mirror waveguides, dielectric waveguides have no absolute cut-off wavelength (or cut-off frequency). A dielectric waveguide can support at least one TE mode, since the fundamental mode $m = 0$ is always supported. Each of the modes $m = 1, 2, \ldots$ has its own cut-off wavelength, however, and the lowest of them determines the conditions for single-mode operation.

Figure 3-2 illustrates the process of selecting the size a of a single-mode Si waveguide and a phase constant β associated with it.

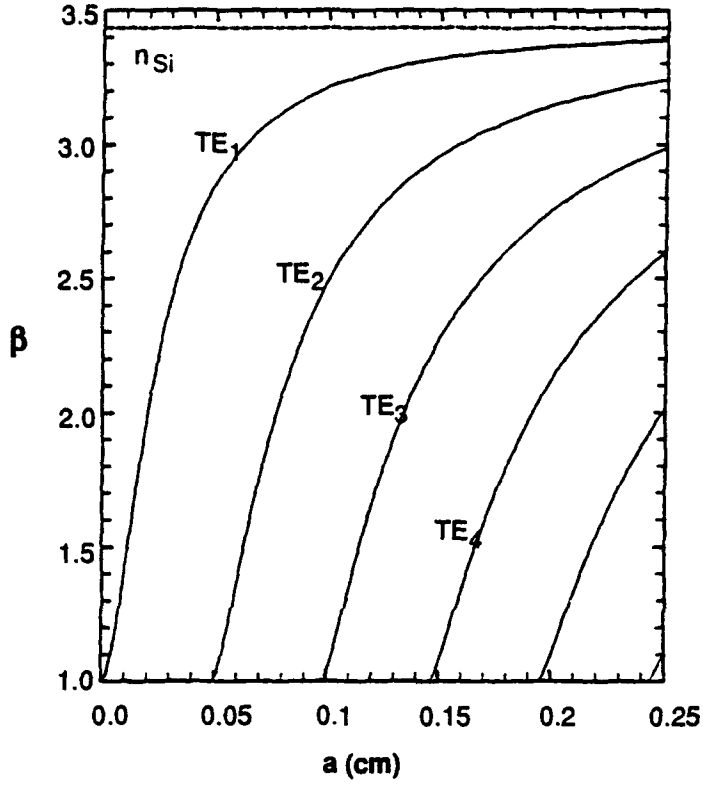

Figure 3-2
TE modes of a Si planar waveguide.

The other dimension of the silicon slab must be close to the internal size of the rectangular mirror waveguide which will deliver MMW power to the silicon slab. For a standard rectangular waveguide with a width-to-thickness ratio of 2 to 1 ($a_1 = 2b_1$), single-mode operation will be preserved if $2a_1 > \lambda_0 > a_1$; the waveguide dimensions are illustrated in Figure 3-3.

From the above mode estimation it follows that a silicon waveguide for single-mode operation at 90 GHz must have a cross section not bigger than 0.48 mm× 1.25 mm. To obtain high coupling efficiency and low beam divergence of the beam radiating from the antenna, the silicon waveguide must have a length of at least several centimeters. Accordingly, a 4-in silicon rod was cut out of a standard Si wafer and further thinned down to the required dimension.

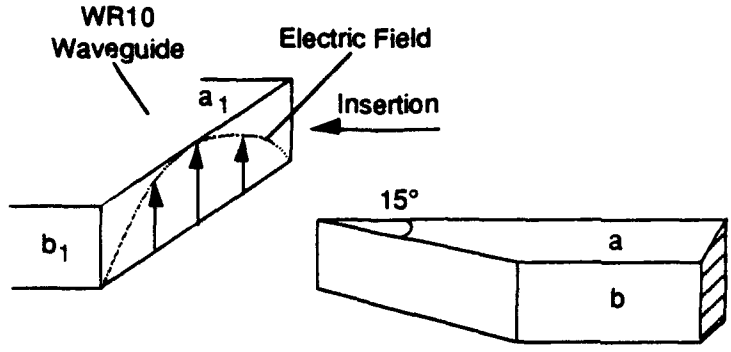

Figure 3-3
Schematic diagram of the waveguide-slab coupler.

The coupling of MMW radiation between the rectangular mirror waveguide and the silicon slab was accomplished by tapering the waveguide, as shown schematically in Figure 3-3. The tapered silicon waveguide was inserted a few millimeters into the mirror waveguide. The other end of the silicon waveguide was also tapered, and was inserted into the output waveguide to form a matched load. We used a standard WR10 (2.54 mm × 1.27 mm) waveguide at 90 GHz as a mirror waveguide.

Waveguide grating couplers are often used as effective replacements for prism couplers in integrated optics. A leaky-wave antenna is the RF counterpart of the grating coupler, although their theoretical treatment is different. Since the light-induced variations in the dielectric permittivity are complex (both real and imaginary parts are affected), GAIL's grating coupler combines the properties of both dielectric and metal leaky-wave antennas.

Periodic dielectric antennas consist of a uniform dielectric waveguide with a periodic surface perturbation. The surface perturbation of the waveguide usually takes the form of a dielectric grating (as shown in Figure 3-4(a)) or a grating of metal strips (as in Figure 3-4(b)).

The waves supported by periodic dielectric antennas radiate as they travel along the antennas; they are leaky-modes which decay exponentially in the forward direction. Of primary interest for antenna applications is the lowest leaky mode. As explained earlier, higher leaky modes can be suppressed by making sure that the antenna dimensions are below the cutoff conditions of these modes or by using an appropriate feed arrangement. If a narrow bandwidth in both principal planes of the antenna is desired, the width of the dielectric waveguide has to be large and single-mode excitation must be ensured by the use of an appropriate feed arrangement.

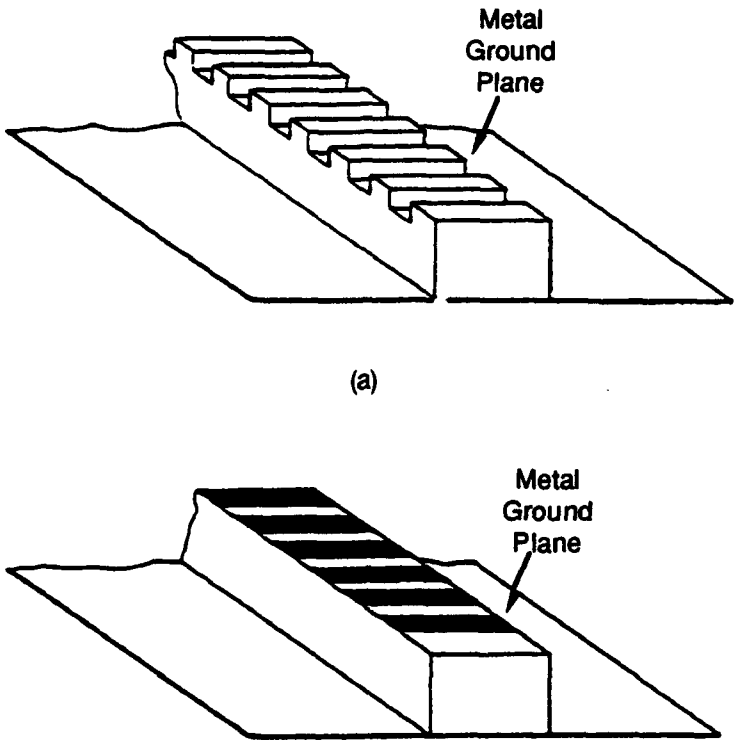

Figure 3-4
Periodic dielectric antennas: (a) antenna with dielectric grating; (b) antenna with metal grating.

A leaky mode can be characterized by a phase constant β and an attenuation, or leakage, constant α, the latter being a measure of the power leaking away per unit length along the antenna. The periodicity produces an infinity of space harmonics associated with that leaky mode. The phase constants β_n of the various space harmonics are related to the phase constant β of the basic wave by $\beta_n = \beta + 2\pi n / D$, $n = 0, \pm 1, \pm 2, \ldots$, where the integer n is the order of the given space harmonic ($n = 0$ corresponds to the basic wave); in this section, D denotes the period of the grating.

The condition for coupling the radiation out of the waveguide using a grating coupler is given by

$$\phi_n = \sin^{-1}(\beta_n / k_0) = \sin^{-1}(\beta / k_0 + n\lambda_0 / D) \quad , \qquad (3\text{-}1)$$

where λ_0 is the free-space wavelength, $k_0 = 2\pi/\lambda_0$ is the free space wave number, and ϕ_n is the radiation angle measured from the normal to the antenna surface (the z axis in Figure 3-5).

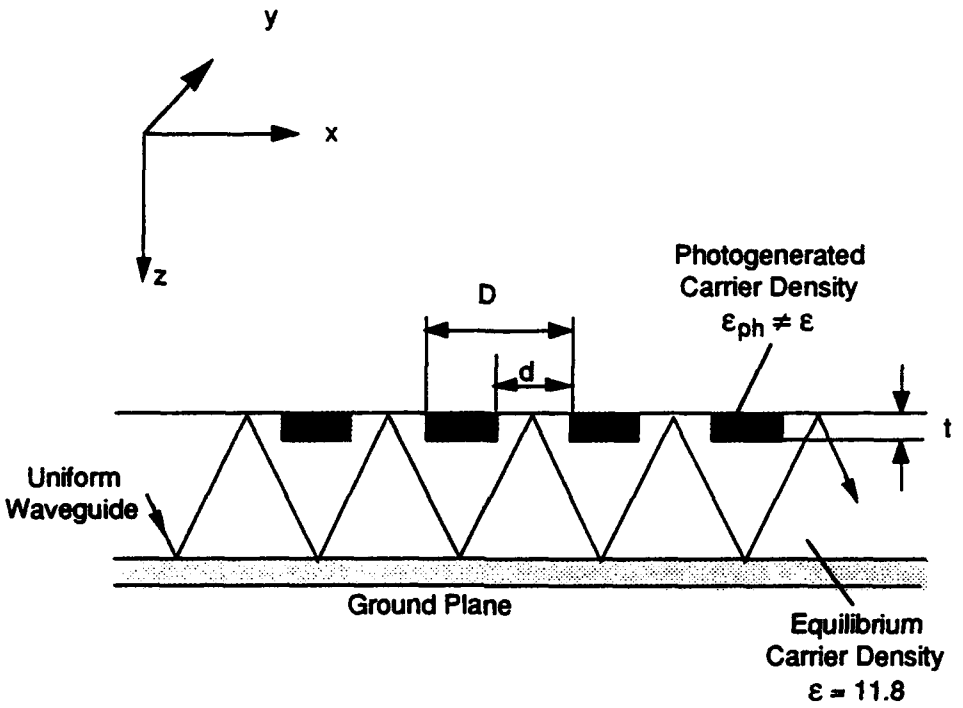

Figure 3-5
Antenna with a periodic perturbation caused by a light-induced grating imposed on the surface of the silicon waveguide.

The number of radiating spatial harmonics depends on the ratio D/λ_0, and is always finite. If D/λ_0 is large, several spatial harmonics propagate into the waveguide and the antenna will radiate in several directions simultaneously. Most antenna applications, however, require single-beam operation, which leads to the following conditions for D [6]:

$$\frac{\lambda_0}{\frac{\beta}{k_0}+1} \leq D \leq \frac{\lambda_0}{\frac{\beta}{k_0}-1}, \text{ for } \frac{\beta}{k_0} > 3$$

$$\frac{\lambda_0}{\frac{\beta}{k_0}+1} < D < \frac{2\lambda_0}{\frac{\beta}{k_0}+1}, \text{ for } \frac{\beta}{k_0} < 3 \quad . \tag{3-2}$$

If these conditions are satisfied, only the n = -1 order spatial harmonic will radiate. The proper waveguide coupler geometry was chosen so that these conditions were met. In addition, internal resonance introduces some leaky-wave stopbands in the radiating angle. They are relatively narrow if the permittivity of the guiding material is high, as it is for silicon ($\varepsilon = 11.8$). Since most practical antennas have a beamwidth of several degrees, the stopband effect will be negligible. For antennas with very narrow beamwidths, a decay of the radiation at these angles may be observed.

In the case of single-beam operation, where only one spatial harmonic is of the radiating type, the radiation properties of the antenna are fully determined by the complex propagation constant $k_x = \beta - i\alpha$. Hence, β and α are the most important parameters to be accounted for by the theory.

The theory underlying the operation of a periodic leaky-wave dielectric antenna with rectangular grooves is presented in Ref. [6]. The theory of a metal-grating antenna appears in Ref. [7]. The leaky-wave dielectric antenna with a photo-induced grating is an intermediate case, where periodic perturbations occur in regions with carrier concentrations much higher than in dielectric materials and much lower than in metals. Therefore, to correctly describe the operation of our antenna requires an adaptation and eventually a merger, of the two theoretical models.

To gain an insight into the efficiency with which an incoming (or outgoing) MMW is coupled into (or out of) the waveguide, we have analyzed the efficiency of a diffraction grating with variable parameters. This modifiable grating is formed by strips of conductive electron-hole plasma created by a properly shaped light illumination pattern on a silicon wafer. This pattern causes diffraction of the incident MMW beam, resulting in the formation of reflected and transmitted diffraction orders. In addition, nonradiating (evanescent) waves are also generated. To a first approximation, the strength of the coupling can be characterized by the sum of the nonradiating waves resulting from the diffraction. Specifically, coupling can be approximated as the difference between the incident MMW radiation and the sum of the reflected and transmitted radiation. Then, the efficiency is defined as the ratio of the power coupled into the substrate to the incident power. An estimation of the grating's efficiency can then be performed within the electromagnetic theory of the grating.

Figure 3-6 shows the wave vectors of the incident wave k_0, reflected wave R_i, transmitted wave T_i, and evanescent diffraction orders E_i ($i = 0, \pm 1, \pm 2, \ldots$). Q is the grating vector. The incident wave is propagating perpendicular to the grating grooves and is polarized along the

grooves, which are oriented along the y-axis. In this case, the diffracted electromagnetic waves, reflected and transmitted, have the same polarization, known as the P-polarization. They are described by the E_y component of the field which satisfies the Helmholtz equation

$$\Delta E_y + \varepsilon(x,z)k_0^2 E_y = 0 \quad , \tag{3-3}$$

and the proper boundary conditions. The grating's thickness, measured along the z-axis, is t. Outside the grating $\varepsilon = 1$.

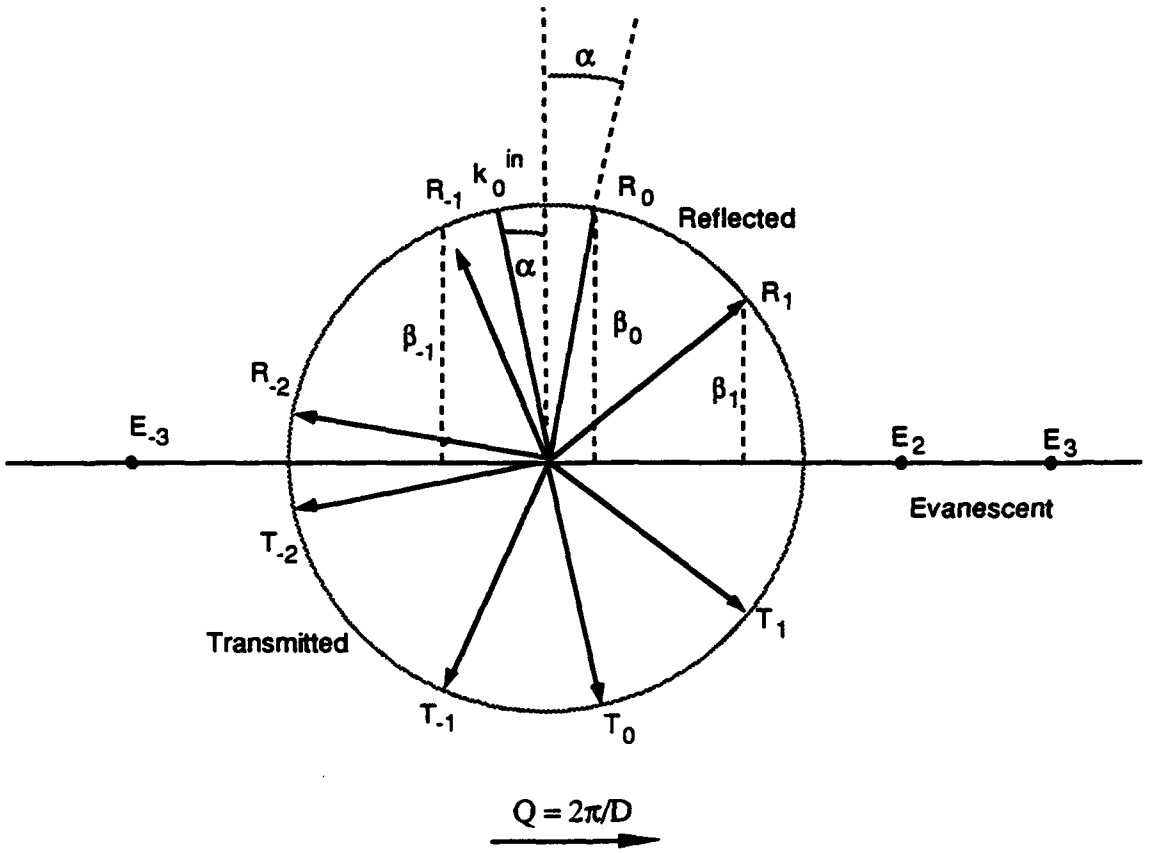

Figure 3-6
Wave vector representation for MMW diffraction.

Inside the grating, the dielectric constant ε is a periodic function of x:

$$\varepsilon(x,z) = \varepsilon(x + D,z) \quad . \tag{3-4}$$

In the proposed model, the dielectric constant ε is a step function of the variable x and an exponentially decreasing function of the variable z. The width of the grooves d and their period D are determined by the illumination pattern. The penetration of the illuminating light into the silicon wafer determines the z dependence of ε.

Let us consider the incident microwave radiation of the selected polarization propagating downwards towards the grating at an angle α with respect to the z-axis (normal to the grating, see Figure 3-6), i.e.,

$$E_y^{in} = E_0 e^{ik_0(x \sin\alpha - z\cos\alpha)} \quad . \tag{3-5}$$

The solutions in the reflection region (superscript r) and the transmission region (superscript t) have the form

$$E_y^{r,t} = e(ik_\alpha x) \sum_{n=-\infty}^{\infty} A_n^{r,t} \exp\left(inQx + i\beta_n^{r,t} z\right) , \tag{3-6}$$

where $k_\alpha = k_0 \sin\alpha$, $Q = 2\pi D^{-1}$, and $\beta_n^2 = k_0^2 - (k_\alpha + nQ)^2$.

Ordinary propagating diffracted waves correspond to $\beta_n^2 > 0$. For these waves, $\beta_n^r > 0$ and $\beta_n^t < 0$. Evanescent diffracted waves correspond to $\beta_n^2 < 0$. These waves stay within the vicinity of the grating, and for them $\Im m\beta_n^r > 0$ and $\Im m\beta_n^t < 0$.

The unknown amplitude coefficients $A_n^{r,t}$ have to be determined by matching the waves given in Eq. (3-6) with a solution of Eq. (3-4) in the grating region $0 < z < t$. Because of the system's periodicity, the solution in that region has a Fourier expansion in the x variable, while the coefficients depend on z:

$$E_y^g = e^{ik_\alpha x} \sum_{m=-\infty}^{\infty} B_m(z) \exp(imQx) \quad . \tag{3-7}$$

Introducing this expansion into Eq. (3-4) and applying the Fourier expansion of the dielectric function

$$\varepsilon(x,z) = \sum_{p=-\infty}^{\infty} \epsilon_p(z)\exp(ipQx) \quad , \tag{3-8}$$

one can obtain an infinite set of coupled ordinary differential equations for the expansion functions $B_n(z)$.

$$\frac{d^2B_n}{dz^2} = (k_\alpha + nQ)^2 B_n - k_0^2 \sum_{m=-\infty}^{\infty} \epsilon_{n-m}(y)B_m \quad . \tag{3-9}$$

A truncation of this infinite set of equations to a finite order is required in a numerical treatment of the problem. The 2(2N + 1) independent solutions of the system of Eq. (3-9) which connect the set of amplitudes $\{B_i\}$ at the grating boundaries at $z = 0$ and $z = t$ are needed to match the required boundary conditions. The boundary conditions must include the incident wave and preserve the continuity of the E_y and H_x fields on both surfaces of the grating. Imposing these conditions, one can determine the diffracted waves' amplitudes A_j^r and A_j^t ($|j| \le N$).

The efficiency $\eta_n^{r,t}$ of the diffracted n-th wave (reflected or transmitted) is

$$\eta_n^{r,t} = \left|A_n^{r,t}\right|^2 \frac{\beta_n^{r,t}}{\beta_0} \quad . \tag{3-10}$$

The dielectric function $\varepsilon(x,z)$ can be found from the Drude model of light-carrier interaction.

The total efficiency Σ of radiation coupling calculated for a Si wafer and a light induced grating with nonequilibrium electron density $N = 5 \cdot 10^{15}$ cm^{-3}, D = 1.5 mm, d = 0.5 mm, and t = 0.55 mm is shown in Figure 3-7.

As can be seen from Figure 3-7, the above theory does predict a resonant coupling that peaks at 44° for the listed parameters. Thus, the theory can be considered as the first step toward an analysis of the optically induced grating coupler.

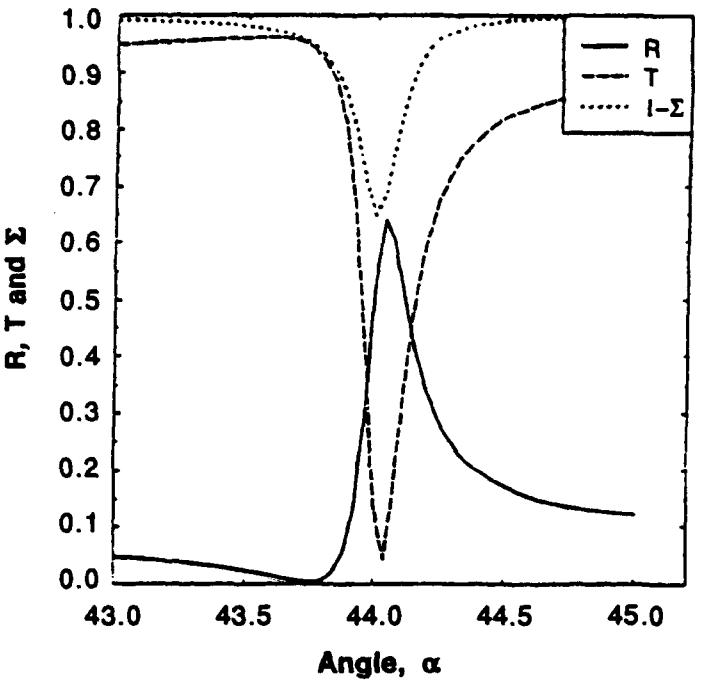

Figure 3-7
Example of the rough calculation of the grating coupling efficiency, Σ (Σ = 1 - R -T).
The theoretical model was further refined in Task 2.

The flexibility of the semiconductor waveguide, where the leakage constant can be controlled by illumination level as well as by choice of an appropriate illumination pattern, allows the antenna design to be optimized.

Another degree of freedom is introduced through the use of pulse illumination. This causes a nonstationary process in the semiconductor, and opens new possibilities for antenna operation. It offers the potential advantages of low power consumption, improved heat balance, and stealth. In addition, a higher grating contrast can be induced by pulse operation than in steady state operation.

3.2 Experiment

Our approach to developing the GAIL is shown in Figure 3-8. To conduct the experiments shown in Figure 3-8, we used a specially prepared 90 GHz test station. The station (see Figure 3-9) is housed in a box lined with material which is highly absorbent in the MMW band. The station includes a high power (80 mW) InP Gunn oscillator, a GaAs Schottky diode as a MMW-radiation detector, corrugated horn antennas, single mode metal waveguides, and terminators. As a

pumping light, we used a xenon flashlamp with a pulse duration variable from 100 to 1 μs and with the spectrum shown in Figure 3-10. This spectrum shows strong peaks in the near IR region, which, as shown in our preliminary study, contributes to pumping efficiency.

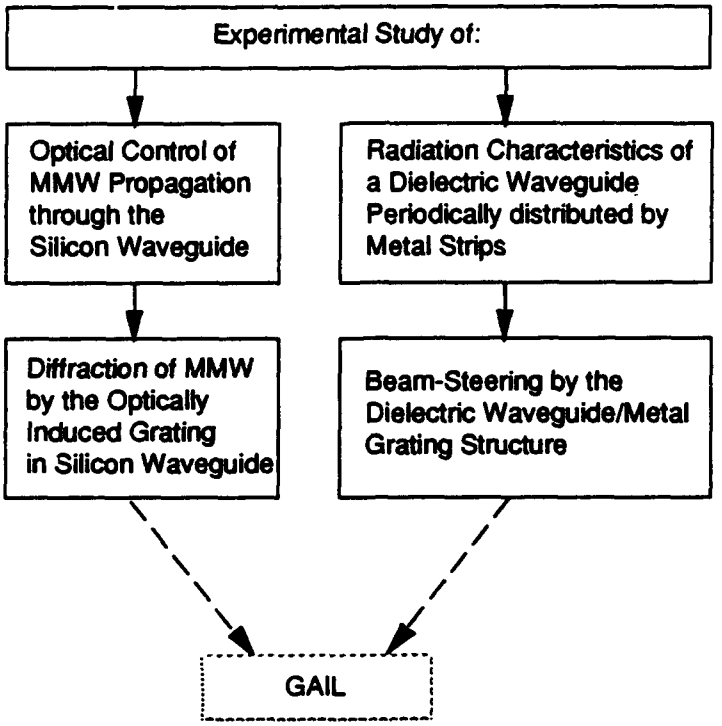

Figure 3-8
Schematic diagram of our experimental study.

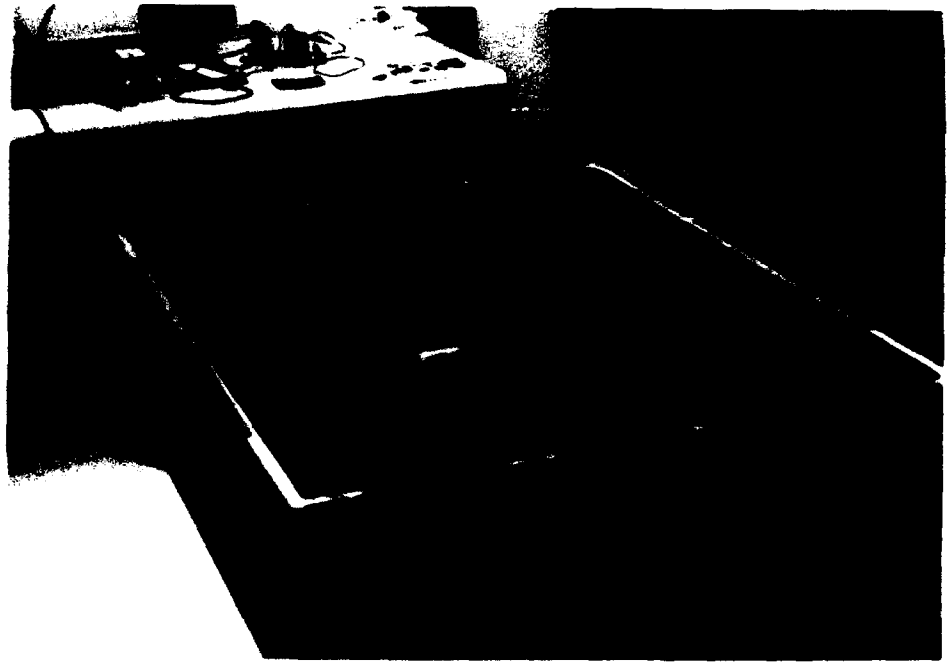

Figure 3-9
POC's MMW equipment in a box with absorbent walls.

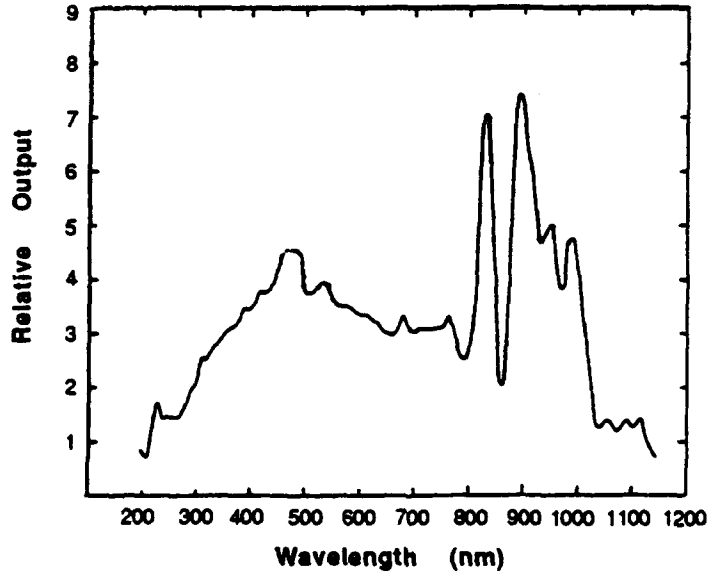

Figure 3-10
Spectrum of light emitted by a xenon flash lamp.

The silicon rod designed for the antenna (see Figure 3-11) was fabricated as follows. High resistivity silicon wafers ($\rho > 10^3$ ohm cm) were polished on both sides down to a thickness of 450 ± 10 μm. Then they were scribed and divided into strips 2 mm wide, as shown in Figure 3-12.

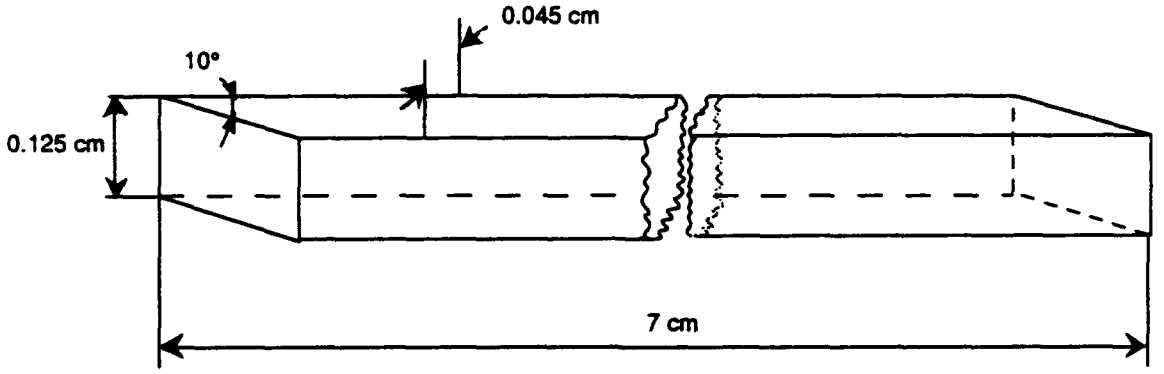

Figure 3-11
Design of silicon rod.

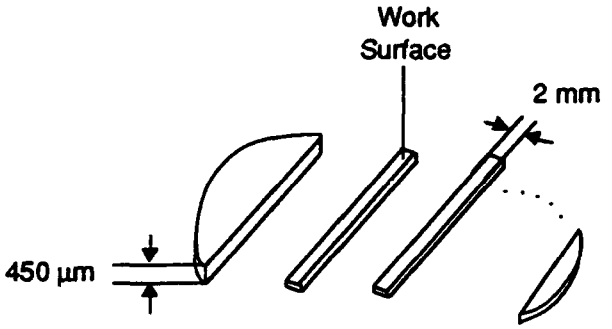

Figure 3-12
Dividing the silicon wafer into strips.

The strips were assembled into stacks and attached to the polishing plate with resin, as shown in Figure 3-13, and then the stack was polished down from both sides to a final thickness of 1.25 mm. After the stack was divided into separate rods, they were attached to a 10° prism and polished from both ends to create a 10° taper for coupling with the metal waveguide. The coupling is shown in Figure 3-14.

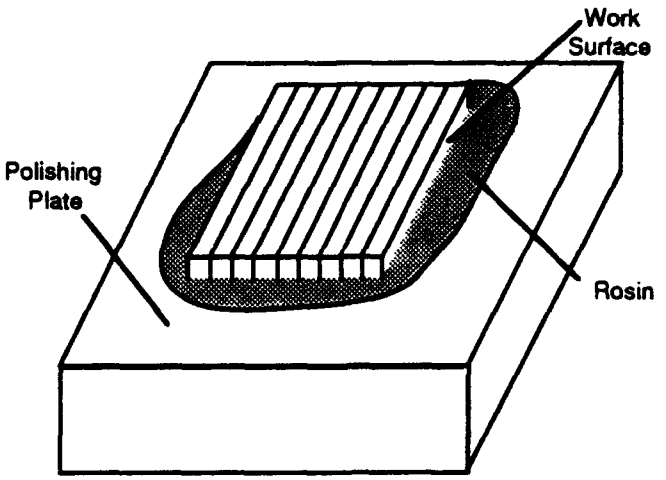

Figure 3-13
Silicon strip set onto the polishing plate.

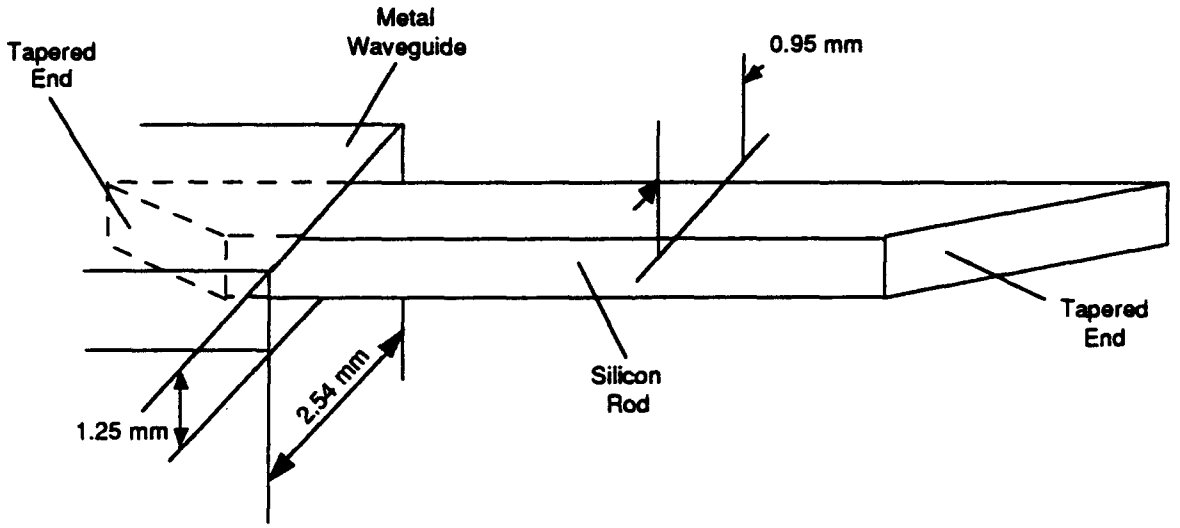

Figure 3-14
Coupling between metal waveguide and silicon rod.

The first experiment studied the optical control of MMW propagation through the waveguide. The experimental setup is shown in Figure 3-15.

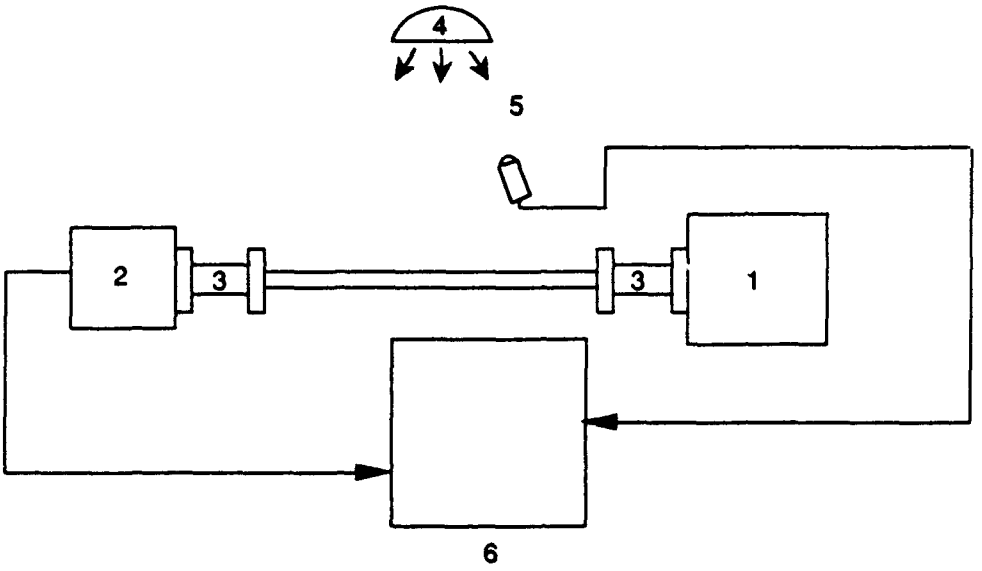

1. Gunn oscillator
2. MMW detector
3. metal waveguides
4. flashlamp
5. Si reflectance photodetector
6. oscilloscope

Figure 3-15
Schematic setup for the study of the MMW propagation through the silicon waveguide under illumination.

The experiment started with optimization of the coupling between the silicon waveguide and the metal waveguides by varying the distance of the silicon waveguide's penetration into the metal waveguide. This procedure was repeated several times to maximize the signal from the detector. Once the coupling was optimized, the study examined the change in MMW propagation under illumination. It was found that interference between MMWs propagating through the silicon waveguide and photo-induced electron-hole plasma is very strong, and that moderate pumping light can saturate the dielectric and block the MMW propagation. This can be seen from Figure 3-16, which shows the pumping light (upper) and propagating MMW intensity (lower).

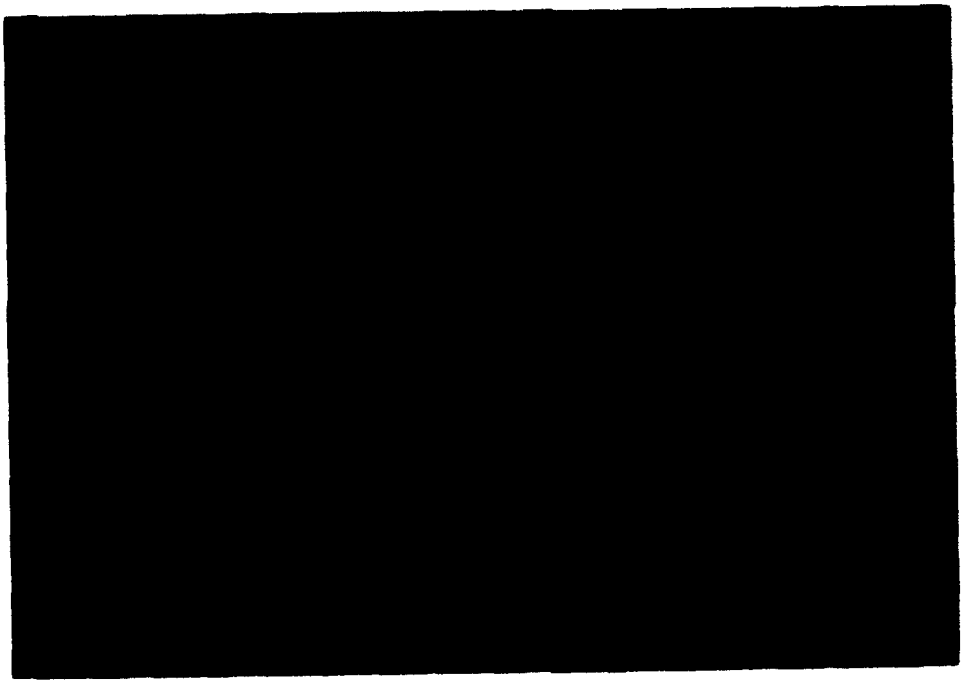

Figure 3-16
Oscillogram of pumping light (upper) and intensity of
MMW propagating through the silicon waveguide (lower).

The bottom line of the oscilloscope grid corresponds to the "zero" intensity of the MMW propagating through the Si waveguide. It can be seen that under illumination the signal is close to 0 (the small variation is caused by detector noise). The duration of the pumping pulse (upper) is much shorter than that of the waveguide response (lower), which reflects a deep saturation of the waveguide by the photo-induced plasma. The transition time between off and on states corresponds to the carrier lifetime in the silicon waveguide at a level of ~80 ms, which is much shorter than in the bulk material the waveguide was made of, showing that surface recombination in this case is much more important than bulk recombination.

The next step was to extract radiation from the silicon waveguide with a photo induced grating. We used the same pumping light, which in this case illuminated the silicon waveguide through a mask that was totally transparent to MMWs. The mask represented an amplitude grating for the pumping light. The experimental setup is shown in Figure 3-17.

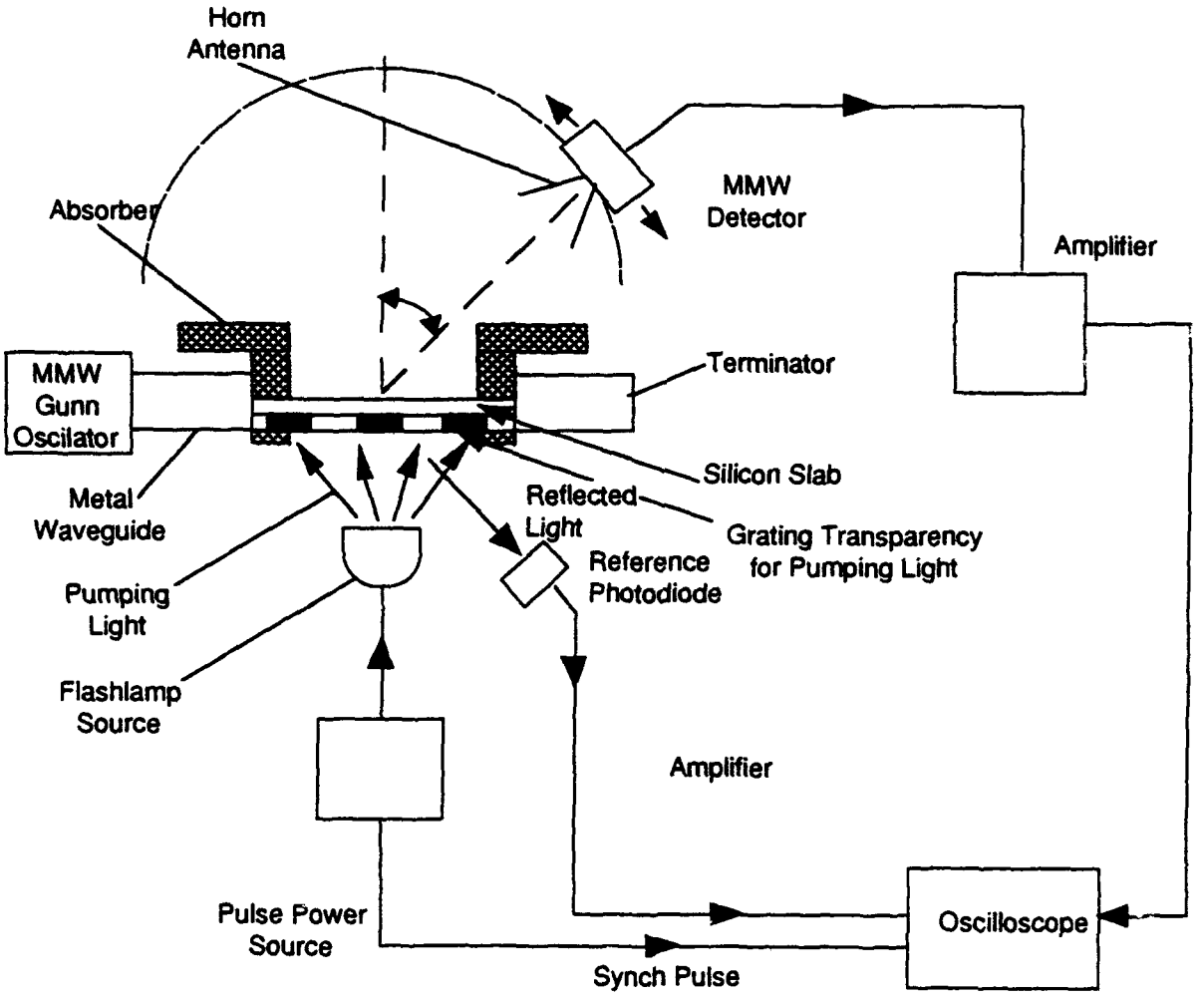

Figure 3-17
Experimental setup for testing GAIL.

In this experiment, the intensity of the pumping light and the position of the detector were varied, but no diffracted MMW beam was detected. The reason for this was the strong interaction between the photo-induced plasma and the MMW radiation propagating through the waveguide. To weaken this interaction, a shorter-wavelength, Ar-laser, pumping light was used which was strongly absorbed by the silicon material. In this case, the photo-induced plasma was generated at the waveguide surface only, and the plasma-MMW interaction was weaker, producing the desired effect.

Another approach was to perturb the MMW not within the waveguide body but in the evanescent field propagating in the closest proximity to the waveguide body. This case is complicated by the presence of several new parameters which had to be taken into account, such as the distance between the photo-induced grating and the waveguide, and by the influence of the grating on the propagating constant.

It is convenient to start the study with a dielectric waveguide perturbed by the metal strips. A silicon-rod antenna whose evanescent waves are perturbed with a metal grating is shown in Figure 3-18.

Figure 3-18
Silicon-rod antenna with metal-strip grating, developed at POC.

The study found that the efficiency of the antenna strongly depends on the width of the metal strips and the distance between them and the silicon rod. To obtain maximum efficiency, this distance is not fixed but is made a function of the running coordinate. The beam pattern radiated by the antenna (see Figure 3-19) corresponds to a 4 degree beam width, which is what it should be, given the radiating length.

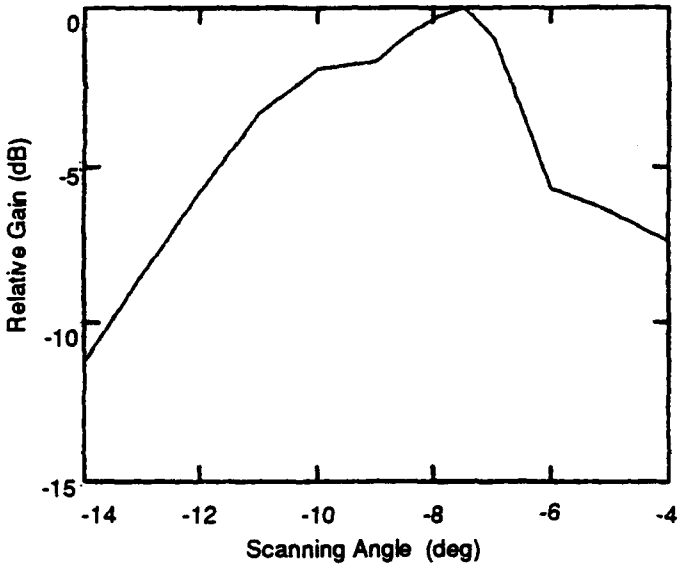

Figure 3-19
Beam pattern produced by the antenna grating coupler.

The results obtained during the dielectric antenna study led to the fabrication of a working laboratory prototype of this extremely cost effective beam-steering antenna (see Figure 3-20).

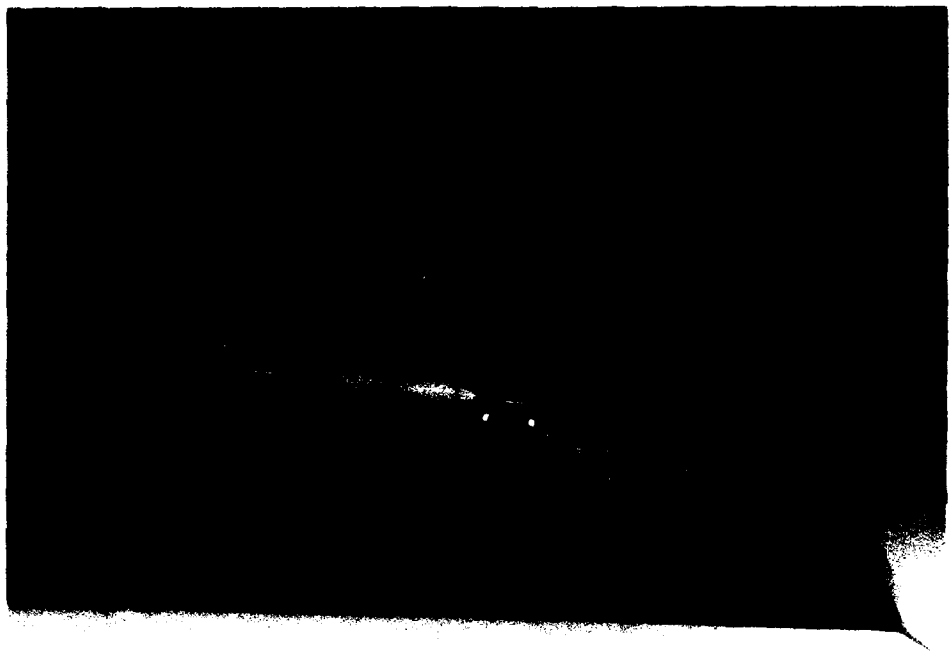

(a)

(b)

Figure 3-20
Beam-steering dielectric-rod antenna with rotating metal-strip grating:
(a) view from rear, and (b) view from above.

In this antenna, a grating with a varying distance between the metal strips (i.e., varying grating period) is mounted on the drum surface, which is rotated at a constant speed. The angle of the radiated MMW beam depends on the grating period and, due to the rotation of the drum, undergoes continuous variation. The oscillogram of the signal detected by the receiving antenna in one fixed direction (in this case it is 30° from the normal) is shown in Figure 3-21.

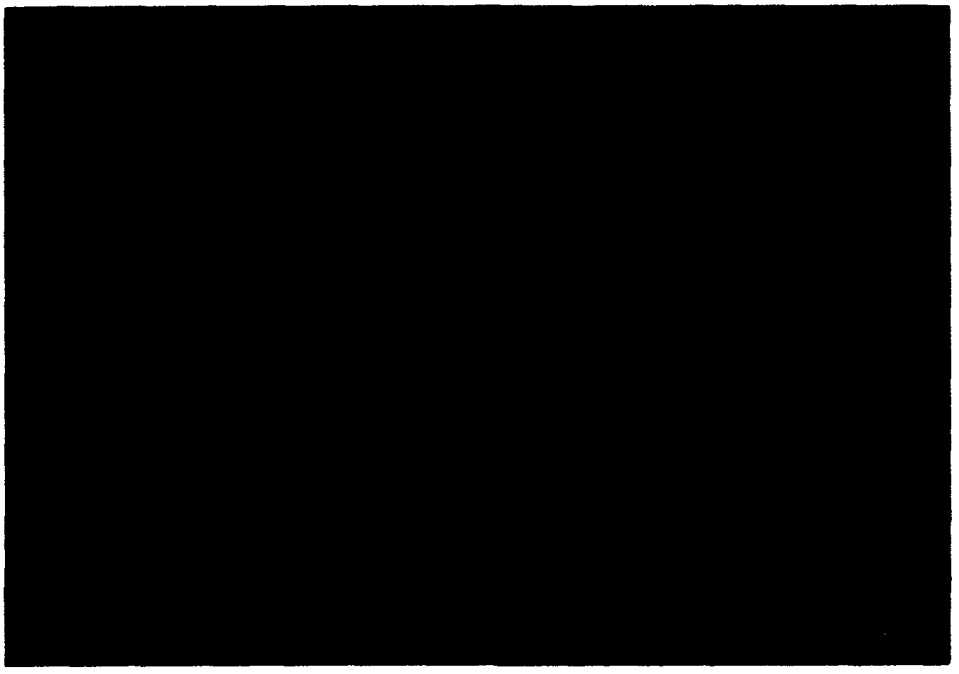

Figure 3-21
MMW pulse radiated by the dielectric rod antenna with rotated grating at 30° from the normal.

4.0 SUMMARY OF THE RESULTS

This research project resulted in:

- Development of a theoretical model of the GAIL
- Demonstration of the use of illumination to control MMW radiation propagating through the silicon rod waveguide
- Establishment of solid theoretical and experimental grounds for further development
- Demonstration of a new type of beam-steering MMW antenna, which is extremely cost-effective and in the near future can be made commercially available.

5.0 REFERENCES

1. Skolnik, M. I., Introduction to Radar Systems. New York: McGraw-Hill (1980).
2. Y. Ayasli, et al., "Wide-Band Monolithic Phase Shifter," IEEE Trans Electron Devices, v. ED-31, (12), pp. 1943-1947 (1984).
3. Harrison Corporation, "Optically Implemented Radio and Radar Functions," Final Technical Report, contract number RADC-TR-90-169 (1990).
4. Rockwell International Science Center, "Optically Implemented Radio and Radar Functions," Final Technical Report, contract number RADC-TR-89-369 (1990).
5. L. Sadovnik, V. Manasson, and T. Jannson, "Light Controlled Spatial and Angular Electromagnetic Wave Modulator", U.S. Patent #818,805 (1994).
6. S. T. Peng and F. Schwering, "Design of Dielectric Grating Antennas for Millimeter Wave Applications," IEEE Trans. Microwave Theory Techn., V. MTT-31, pp. 199-209 (1983).
7. M. Gugliemi and A. A. Oliner, "A Practical Theory for Image Guide Leaky-Wave Antennas Loaded by Periodic Metal Strips," Proc. 17th European Microwave Conference pp. 549-554 (1987).